

A probabilistic approach to characterizing drought using satellite gravimetry

Peyman Saemian¹, Mohammad J. Tourian¹, Omid Elmi¹

Nico Sneeuw¹, Amir AghaKouchak^{2,3}

¹Institute of Geodesy, University of Stuttgart, Stuttgart, Germany

²Department of Civil and Environmental Engineering, University of California, Irvine, CA, USA.

³United Nations University Institute for Water, Environment and Health, Hamilton, Ontario, Canada

Key Points:

- A probabilistic framework is introduced to characterize drought using GRACE and GRACE Follow-On observations.
- Our study highlights a tendency of deterministic approaches to consistently overestimate storage-based drought severity.
- The probabilistic approach captures global droughts while delivering more realistic results suited for risk management.

Corresponding author: Peyman Saemian, peyman.saemian@gis.uni-stuttgart.de

Abstract

In the recent past, the Gravity Recovery and Climate Experiment (GRACE) satellite mission and its successor GRACE Follow-On (GRACE-FO), have become invaluable tools for characterizing drought through measurements of Total Water Storage Anomaly (TWSA). However, the existing approaches have often overlooked the uncertainties in TWSA that stem from GRACE orbit configuration, background models, and intrinsic data errors. Here we introduce a fresh view on this problem which incorporates the uncertainties in the data: the Probabilistic Storage-based Drought Index (PSDI). Our method leverages Monte Carlo simulations to yield realistic realizations for the stochastic process of the TWSA time series. These realizations depict a range of plausible drought scenarios that later on are used to characterize drought. This approach provides probability for each drought category instead of selecting a single final category at each epoch. We have compared PSDI with the deterministic approach (SDI) over major global basins. Our results show that the deterministic approach often leans towards an overestimation of storage-based drought severity. Furthermore, we scrutinize the performance of PSDI across diverse hydrologic events, spanning continents from the United States to Europe, the Middle East, Southern Africa, South America, and Australia. In each case, PSDI emerges as a reliable indicator for characterizing drought conditions, providing a more comprehensive perspective than traditional deterministic indices. In contrast to the common deterministic view, our probabilistic approach provides a more realistic characterization of the TWS drought, making it more suited for adaptive strategies and realistic risk management.

Plain Language Summary

Total Water Storage (TWS) is defined as the sum of water stored as surface water (e.g., lakes and rivers), groundwater, soil moisture, snow, ice, and vegetation biomass. Since its launch in 2002, the Gravity Recovery and Climate Experiment (GRACE) satellite mission has provided unique TWS change measurements with manifold applications in hydrology,

41 including characterizing drought events. Scientists have been using satellites like GRACE
42 and its successor, GRACE-FO, to understand drought by measuring the Total Water Storage
43 Anomaly (TWSA). However, previous methods didn't consider uncertainties from satellite
44 orbits, models, and data errors. This study offers a novel probabilistic approach for char-
45 acterizing drought, Probabilistic Storage-based Drought Index (PSDI), which acknowledges
46 the uncertainties in the GRACE TWS change. We use simulations to create different drought
47 scenarios, offering probabilities for each category instead of one fixed category. Compar-
48 ing PSDI to traditional methods, we found that traditional methods tend to overestimate
49 drought severity. We tested PSDI across different regions, and it consistently proved to be a
50 reliable way to understand drought conditions, offering a more comprehensive perspective.
51 Our probabilistic approach offers a more realistic view of TWS drought, making it suitable
52 for adaptive strategies and risk management.

53 **1 Introduction**

54 The modern reality of human settlement is the consequence of many historical events, but
55 perhaps none influenced human settlements as much as droughts and famine. DNA analysis
56 indicates that a series of extreme droughts that occurred 75-135 thousand years ago may
57 have been the reason for the first human migration out of Africa (Scholz et al., 2007).
58 Following several consequential droughts over the past century (e.g., the 1921 drought in
59 Europe, the 1930s Dust Bowl drought in the US, 1928-1930 drought in China, 1980s drought
60 and famine in Africa, 2000s Millennium drought in Australia), increasingly more effort has
61 focused on understanding, monitoring and predicting droughts and their impacts (Mishra
62 & Singh, 2010; Heim Jr, 2002; AghaKouchak et al., 2015; Svoboda et al., 2002; Wilhite et
63 al., 2007; Kreibich et al., 2022; AghaKouchak et al., 2021).

64 Compared to other hazards witnessed over the past four decades, drought impacts are often
65 felt by a much larger number of people worldwide (Wilhite, 2000; FAO, 2021; AghaKouchak
66 et al., 2021). Numerous nations have grappled with significant economic losses resulting

67 from drought events. Notably, according to the NOAA's National Centers for Environmental
68 Information (NCEI) report, the United States has experienced 26 significant droughts in the
69 past century, amounting to a staggering economic loss of at least \$249 billion, equivalent
70 to nearly \$10 billion per occurrence. In Europe, the southern and western regions, in
71 particular, face an annual drought-related expenditure estimated at up to €9 billion, which
72 could surge to over €65 billion if climate action is not taken (Naumann et al., 2021). Aside
73 from the financial burdens, climate change, and unsustainable water management practices
74 have amplified the frequency and severity of drought occurrences worldwide over the past
75 two decades. This trend is projected to escalate further in the future (see e.g., Hisdal et al.,
76 2001; Coumou & Rahmstorf, 2012; Yu et al., 2014; Donat et al., 2016; Teuling, 2018; Li et
77 al., 2021; C. Zhao et al., 2020).

78 The negative consequences of drought can be effectively alleviated through the implemen-
79 tation of risk management strategies rather than relying on crisis management (Wilhite,
80 2000; Zscheischler et al., 2018). Such a proactive response may be achieved by establishing
81 reliable drought monitoring systems, including early warning systems and forecasting capa-
82 bilities, operating at both national and local levels (Wilhite et al., 2007; AghaKouchak et al.,
83 2023). These systems trigger a series of decisions aimed at helping communities navigate the
84 challenges posed by drought events (Mishra & Singh, 2011; Sun et al., 2017). To enhance
85 drought monitoring efforts and provide valuable guidance to decision-makers, numerous
86 drought indices have been developed (Mishra & Singh, 2010). These indices condense the
87 intricacies of drought into a single numerical value, effectively characterizing its onset, in-
88 tensity, frequency, and duration (Zargar et al., 2011; Wilhite, 2000; Ahmadalipour et al.,
89 2017). Such indices offer a comprehensive representation of drought by utilizing single or
90 multiple climatic and hydrometeorological variables such as precipitation, streamflow, evap-
91 otranspiration, temperature, and snowpack (e.g., Svoboda et al., 2016; Hosseini-Moghari et
92 al., 2020).

93 A comprehensive understanding of drought dynamics necessitates the observation of Total
94 Water Storage (TWS) including snow, surface water, soil moisture, and groundwater storage
95 (M. Zhao et al., 2017; M. J. Tourian et al., 2023). Traditionally, TWS monitoring has
96 relied on costly and time-consuming site measurements, providing limited regional and local
97 coverage. While hydrological and land surface models partially address this issue, estimating
98 TWS in regions lacking in-situ runoff data for calibrating rainfall-runoff models still yields
99 high uncertainties (Jiang et al., 2014; S. Yi et al., 2023). Since its launch in 2002, the Gravity
100 Recovery And Climate Experiment (GRACE) satellite mission has revolutionized the remote
101 measurement of TWS Anomalies (TWSA) at regional to continental scales (Tapley et al.,
102 2004; M. J. Tourian et al., 2022). The GRACE mission came to an end on 12 October 2017,
103 due to battery failure, after more than 15 years of Earth observation. However, its successor,
104 GRACE Follow-On (GRACE-FO), has continued the GRACE legacy since its launch on 22
105 May 2018. GRACE(-FO) data have been extensively utilized for manifold applications,
106 including monitoring ice sheets and glaciers (e.g., van den Broeke et al., 2009; Gardner et
107 al., 2013; Shepherd et al., 2018), tracking anthropogenic groundwater depletion (e.g., Rodell
108 et al., 2007, 2009; Famiglietti et al., 2011; Voss et al., 2013; Saemian et al., 2022), forecasting
109 flood events (e.g., Reager & Famiglietti, 2009; Gouweleeuw et al., 2018), and quantifying
110 and comprehending hydrological processes (e.g., Lorenz et al., 2014; Saemian et al., 2020;
111 M. Tourian et al., 2018; Behling et al., 2022), to name but a few.

112 GRACE-derived estimates of TWS have been employed in developing indices aimed at
113 assessing drought on a regional to global scale. For example, Yirdaw et al. (2008) developed
114 the Total Storage Deficit Index (TSDI), utilizing the Palmer Drought Severity Index (PDSI;
115 Palmer, 1965) and the Soil Moisture Deficit Index (SMDI; Narasimhan & Srinivasan, 2005),
116 to characterize the Canadian Prairie droughts of 2002/2003. Another notable endeavor by
117 Thomas et al. (2014) presented a comprehensive framework for drought characterization
118 based on GRACE-derived TWSA over regions including the Amazon, Zambezi, Texas, and
119 the southeastern United States. Additionally, H. Yi & Wen (2016) devised the GRACE-
120 based Hydrological Drought Index (GHDI) to characterize drought in the continental United

121 States from 2003 to 2012, building upon the foundation of the PDSI concept. Among recent
122 indicators we can name the Drought Severity Index (DSI) by M. Zhao et al. (2017), the
123 Water Storage Deficit Index (WSDI) by Sinha et al. (2017), and a long-term standardized
124 GRACE reconstructed TWSA index (SGRTI) by Zhong et al. (2023).

125 The indices mentioned above have the potential for monitoring and assessing the TWS
126 drought at regional to global scales. Nevertheless, they adopt a deterministic approach that
127 disregards the intrinsic uncertainties associated with characterizing drought using GRACE
128 observations. These uncertainties are inherent in the GRACE data due to factors such as its
129 orbit configuration, measurement concept, various post-processing approaches of GRACE
130 data, and different options for de-aliasing products. Besides, the estimation of GRACE
131 uncertainty varies among different GRACE level-2 products, in both magnitude and spatial
132 pattern. Most of the centers offer an uncertainty measure (known as formal errors) in
133 the form of spherical harmonic coefficients. Figure 1 shows the coefficient-wise ratio of
134 average formal errors and empirical errors of the GRACE solution following the approach
135 suggested by Kvas et al. (2019). The ideal ratio is set at one, with values below indicating an
136 underestimation of empirical errors, whereas values exceeding one signify an overestimation.
137 The three official centers (JPL, CSR, and GFZ) together with AIUB, HUST, and SWPU
138 exhibit a similar pattern. The SWPU solution demonstrates a pronounced overestimation
139 of formal errors, particularly for low d/o (under 30). ITSG and Tongji display comparable
140 patterns, although Tongji tends to lean slightly towards a more pessimistic estimation of
141 errors. In contrast, COST-G reflects more realistic formal errors in comparison to empirical
142 errors but appears overly optimistic for lower d/o values. The distinctive pattern observed
143 in the CNES product can be attributed to the regularization applied during the derivation
144 of the gravity field from the Level-1 dataset. The disparities in formal error performance
145 among GRACE Level-2 products underscore the inherent uncertainty in GRACE data and
146 consequently, the necessity for a comprehensive approach that effectively considers GRACE
147 uncertainty while characterizing drought.

148 To address this gap in conventional methods, we propose a probabilistic approach that
 149 considers all possible scenarios and associated impacts. Our approach leverages Monte Carlo
 150 simulations to obtain realistic realizations of TWSA compatible with GRACE-TWSA and
 151 its corresponding uncertainties. We then characterize drought based on TWSA using our
 152 proposed drought index, the Probabilistic Storage-based Drought Index (PSDI). This index
 153 indicates not only drought but also its corresponding occurrence probability. We compare
 154 our results with those from the conventional deterministic approaches over the major river
 155 basins. Moreover, the performance of PSDI in capturing the main hydrological drought
 156 extremes is examined within the GRACE era. PSDI facilitates more informed and proactive
 157 responses to water resource challenges and serves as a practical tool for decision-makers and
 158 water resource managers to assess and manage drought-related risks more realistically.

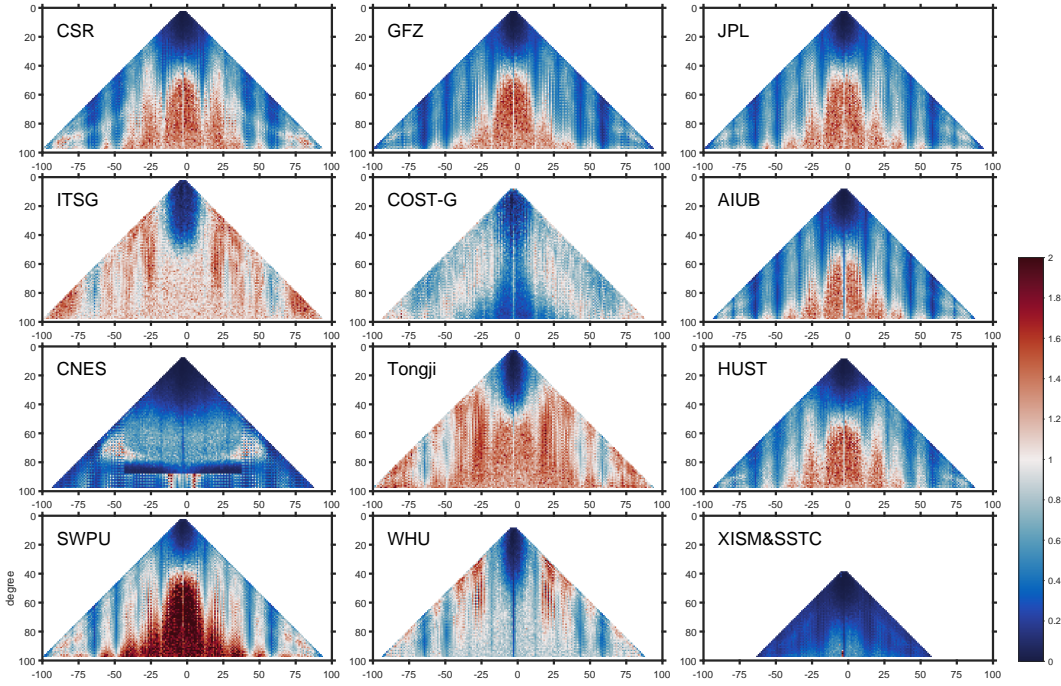


Figure 1. The coefficient-wise ratio of average formal errors and empirical errors of the GRACE solutions following the approach suggested by Kvas et al. (2019). For the average formal errors, the mean of the reported variance of the spherical harmonics coefficients is computed for monthly solutions from January 2005 to December 2010, which is assumed to hold a homogeneous data quality. To estimate the empirical errors, we compute the standard deviation of the coefficients after removing the mean, linear trend, and annual and semi-annual signals. The optimal value of the ratio is one, and values below one indicate an underestimation of the empirical errors, while values bigger than one show overestimation. We have only included solutions that provide formal errors.

2 Data and Method

2.1 GRACE data

The GRACE TWSA can be obtained from the two main approaches, namely Spherical Harmonics (SHs) and mass concentration blocks (mascons). In the former, one needs to apply post-processing steps including noise reduction and signal restoration while the latter is already the Level-3 product (gridded TWSA over the globe). These approaches are briefly described in section 1 of the supplementary file. In line with the common practice within the hydrology community, we have utilized the mascons solutions. The probabilistic approach for characterizing storage-based drought index, however, can readily be applied to any level-3 products that provide estimations for GRACE TWSA and its corresponding uncertainty. Among the mascon products, we have employed the one from Goddard Space Flight Center (GSFC), NASA. The GSFC mascon product has been widely used in the geodesy and Earth science communities to investigate a range of phenomena, including hydrology, glaciology, and solid Earth dynamics, and can be downloaded from <https://earth.gsfc.nasa.gov/geo/data/grace-mascons>. We used the latest version of the dataset available at the time of our analysis, which covers the period from August 2002 to November 2022. The dataset includes monthly gravity field solutions with a grid size of 0.5° .

2.2 Methodology

We propose a probabilistic framework to characterize storage-based drought. The framework is illustrated in Figure 2, Figure 3, and Figure 4 using TWSA over the Death Valley basin in the US as an example. To characterize drought, we must first define a reference, based on which a prolonged relative water deficiency is determined. It is common to consider the long-term monthly average, also known as the *climatology*, as the reference or *normal* condition in a region. Obtaining accurate climatology from short time series can be challenging. Calculating the climatology over at least 30 years, preferably 60 years, is standard practice, as this time frame allows us to average out the effects of short-term variability, resulting

185 in a more robust estimate of the long-term average conditions (e.g., Hulme, 1992; Jones &
 186 Hulme, 1996; Svoboda et al., 2012). The GRACE and GRACE-FO missions, with their
 187 approximately 20-year duration, fall short of providing sufficient data for calculating long-
 188 term climatology. In this study, we utilized a combination of different models to estimate
 189 TWSA dating back to 1980. To this end, we incorporated a total of 13 state-of-the-art
 190 datasets including Global Hydrological Models (GHMs), Land Surface Models (LSMs), and
 191 atmospheric reanalysis models. To combine models, we employed the Multivariate Linear
 192 Regression (MLR) method. We compared the results of Multiple Linear Regression (MLR)
 193 in reconstructing TWSA with GRACE time series (see Supplementary section 2). The MLR
 194 exhibits a strong capability to capture the features and effectively reconstruct TWSA data
 195 as far back as 1980. It demonstrated superior performance compared to the ensemble mean
 196 of the models, as indicated by a substantial improvement in both the correlation coefficient
 197 (on average from 0.87 to 0.97) and the Kling-Gupta Efficiency (KGE) score (on average from
 198 0.27 to 0.95) across major river basins. For more details about the datasets and long-term
 199 TWSA, please refer to Supplementary section 2. This extended time frame enables us to
 200 capture significant climate events and phenomena that influence long-term climate, such as
 201 the El Niño-Southern Oscillation (ENSO) and the North Atlantic Oscillation (NAO) (Sohn
 202 et al., 2013; Coelho & Goddard, 2009).

203 The climatology, along with its corresponding uncertainty (see Figure 2 (a)), is obtained by:

$$\overline{\text{TWSA}}[t_m] = \frac{1}{N} \sum_{y=y_1}^{y_N} \text{TWSA}[t_{y,m}] \quad (1)$$

$$\sigma_{\overline{\text{TWSA}}[t_m]}^2 = \frac{1}{N} \sqrt{\sum_{y=y_1}^{y_N} \sigma_{\text{TWSA}[t_{y,m}]}^2} \quad (2)$$

204 where $\overline{\text{TWSA}}[t_m]$ represents the TWSA climatology for month m , y denotes the year and can
 205 vary from y_1 to y_N , m corresponds to the month within a year, taking values 1, 2, 3, ..., 12,

206 and N is the number of years in the long-term dataset. Note that we deliberately retain
 207 the trend in the time series. We reason that the trend reflects long-term changes in climate,
 208 such as temperature increases or precipitation pattern alterations, and that it affects the
 209 frequency and severity of droughts (see Supplementary section 3 for more details). We then
 210 subtract the climatology from the GRACE TWSA time series to obtain TWS residual (S):

$$S[t_{y,m}] = \text{TWSA}[t_{y,m}] - \overline{\text{TWSA}}[t_m] \quad (3)$$

$$\sigma_{S[t_{y,m}]} = \sqrt{\sigma_{\text{TWSA}[t_{y,m}]}^2 + \sigma_{\overline{\text{TWSA}}[t_m]}^2} \quad (4)$$

211 where negative values of S represent water storage deficits.

212 To reduce the effects of short-term fluctuations due to precipitation and other factors, we
 213 chose to use a 3-month moving average to smooth the TWS residual (see Figure 2 (b)):

$$S[t] = f * S[t]_{\text{unsmoothed}} \quad (5)$$

214 where $*$ denotes the convolution operation, and f is the kernel $[1/3, 1/3, 1/3]$ which is
 215 convolved with the $S[t]_{\text{unsmoothed}}$ time series.

216 To address the inherent uncertainty, it becomes essential to employ a stochastic approach
 217 that incorporates S along with its associated uncertainty. At each epoch, we postulate a
 218 normal distribution with the mean being the obtained TWS residual $S[t]$ and $\sigma = \sigma_{S[t]}$.
 219 Sampling from this distribution in each time step allows us to create realizations of the S
 220 time series. Several methods exist for sampling from a Gaussian distribution, and one widely
 221 used technique is the Box-Muller transform (Box & Muller, 1958). This method guarantees
 222 generating a realization of S , which is independent epoch-wise with no artificial correlations.
 223 We then use Monte Carlo Simulation (Mooney, 1997; Metropolis & Ulam, 1949) to generate

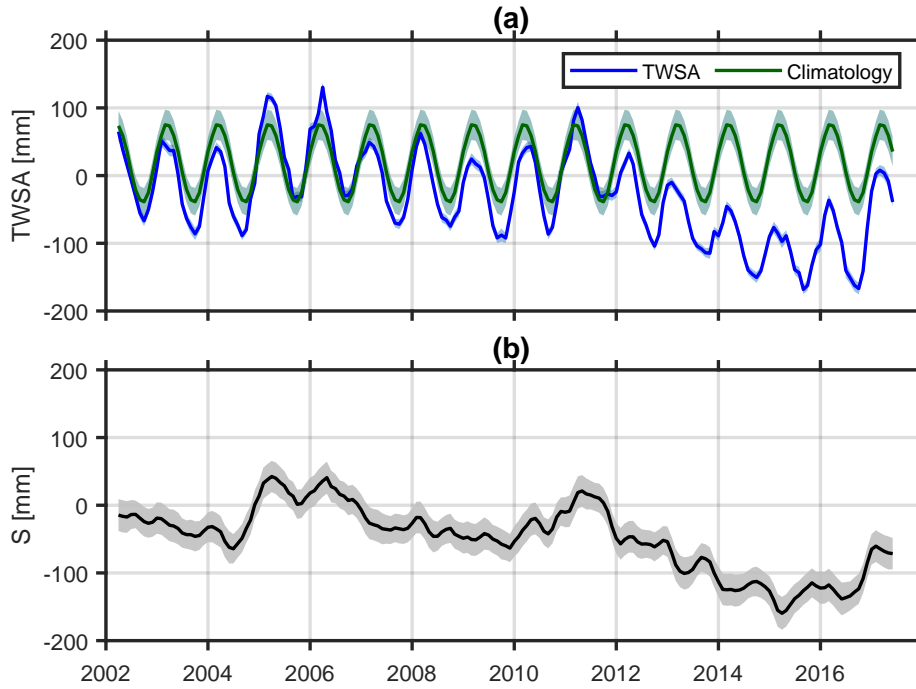


Figure 2. (a) Time series of the long-term TWSA from GRACE and the long-term climatology (1980–2012) from the hindcasted TWSA together with their uncertainties. At each epoch, we assume a Gaussian distribution for the uncertainties and the depicted uncertainty corresponds to the $1\text{-}\sigma$ level. Here the results are shown for the Death Valley basin in the US.

224 multiple realizations of S . Figure 3 shows 10 000 realization of TWS residual considering
 225 the $3\text{-}\sigma$ uncertainty. The density of the realizations is highest around the mean signal and
 226 decays following a Gaussian distribution. The colored lines overlaid on the time series depict
 227 the distribution of outcomes for three specific epochs: July 2004, May 2013, and April 2015.

228 To characterize drought within each time epoch, one common approach is to use the per-
 229 centile rank method and the U.S. Drought Monitor (USDM) criteria. To this end, a set of
 230 five drought categories is defined (Table 1).

231 The quantile values for the S time series can be extracted as the inverse of the Cumulative
 232 Distribution Function (CDF), also known as the quantile function:

$$Q(p) = F^{-1}(p) \quad (6)$$

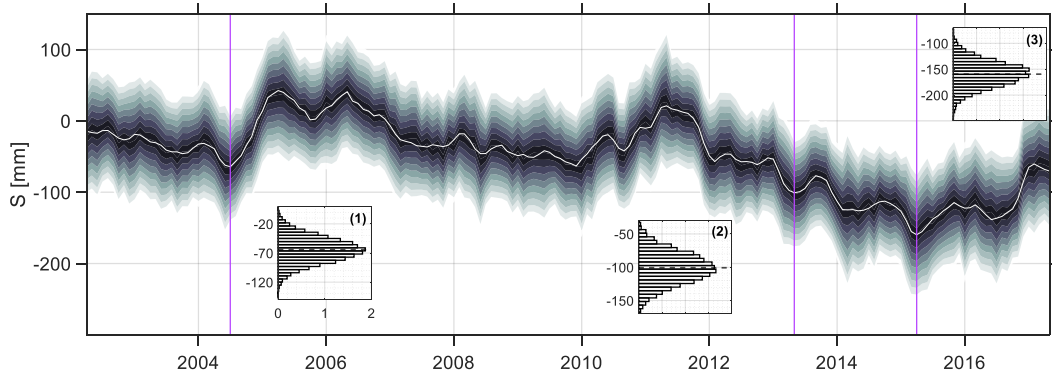


Figure 3. The TWS residual (S) together with its 10 000 realizations, calculated using Monte Carlo simulation. Here the results are shown for the Death Valley basin in the US. The distribution of realizations for three epochs, namely July 2004, May 2013, and April 2015 are marked with colored dots over the time series and are shown in sub-figures.

Table 1. Drought categories and corresponding percentile ranges as defined by the U.S. Drought Monitor (USDM).

Drought Category	Description	Percentile Range
D0	Abnormally dry	20–30%
D1	Moderate drought	10–20%
D2	Severe drought	5–10%
D3	Extreme drought	2–5%
D4	Exceptional drought	Less than 2%

233 where $Q(p)$ represents the quantile function and $F^{-1}(p)$ denotes the inverse CDF evaluated
 234 at probability p . In a conventional deterministic approach, the drought category for each
 235 epoch is determined based on its quantile value of S . For example in Figure 4 (a), the dark
 236 solid line represents the quantile function of the S time series. Using such a function one
 237 can characterize drought for case (1), case (2), and case (3) as D4, D1, and no drought,
 238 respectively.

239 Such an approach overlooks the uncertainty in TWS residual S . However, accounting for
 240 uncertainty would entail obtaining the quantile function for all realizations of S . These
 241 functions form a cloud of points rather than a single line as it has been illustrated in Fig-
 242 ure 4 (a). The quantile functions are shown in grayscale representing the probability $\Pr(p, S)$
 243 for a given percentile p and TWS residual S . Already at this stage, a glance at Figure 4 (a)
 244 reveals the complexity introduced by the uncertainty envelope, challenging the conventional

245 approach to assigning a specific class to a particular measurement. It is noteworthy that the
 246 uncertainty envelope depicted in Figure 4 (a) exhibits a stationarity character, indicating
 247 general uncertainty in the data regardless of the specific time of measurements. This char-
 248 acteristic is reflective of the general uncertainty of S , emphasizing the broader statistical
 249 context rather than being tied to specific instances in time.

250 Now, let's delve into the characterization of drought for one of the measurements illustrated
 251 in Figure 3. In this context, alongside the consideration of the stationary uncertainty as re-
 252 flected in the quantile envelope and represented by $\Pr(p, S)$, it becomes essential to account
 253 for the uncertainty associated with the measurement at that specific epoch. This is funda-
 254 mentally crucial because two GRACE measurements with the same value of S may exhibit
 255 varying levels of uncertainty. Therefore, we incorporate the probability density function of
 256 the value S_t , denoted by $f(S_t)$, obtained from the mean and uncertainty of that epoch.
 257 $f(S_t)$ is shown for the three sample epochs on the top right panel of Figure 4. At each
 258 epoch, we multiply this probability density function with the entire distribution $\Pr(p, S)$,
 259 as illustrated in Figure 4 (c). Essentially, this multiplication results in a down-weighting of
 260 probabilities located in the tails of $f(S_t)$.

261 Once $\Pr(p, S) f(S_t)$ is achieved, to obtain PSDI at each epoch and for each drought category
 262 D_i , we can integrate the probabilities both in S and p domains and normalize it with the
 263 integral over the entire domain:

$$\text{PSDI}(t, D_i) = \frac{\int_S \int_{D_i} \Pr(p, S) f(S_t) dp ds}{\int_S \int_0^1 \Pr(p, S) f(S_t) dp ds} \quad (7)$$

264 By performing this process for all drought categories and time epochs, we generate a com-
 265 prehensive probabilistic representation of drought severity over time. For decision-making
 266 purposes, the highest-probability category can be judiciously chosen as the definitive drought
 267 classification for a particular month. The flowchart of the proposed probabilistic approach
 268 is shown in Figure 5.

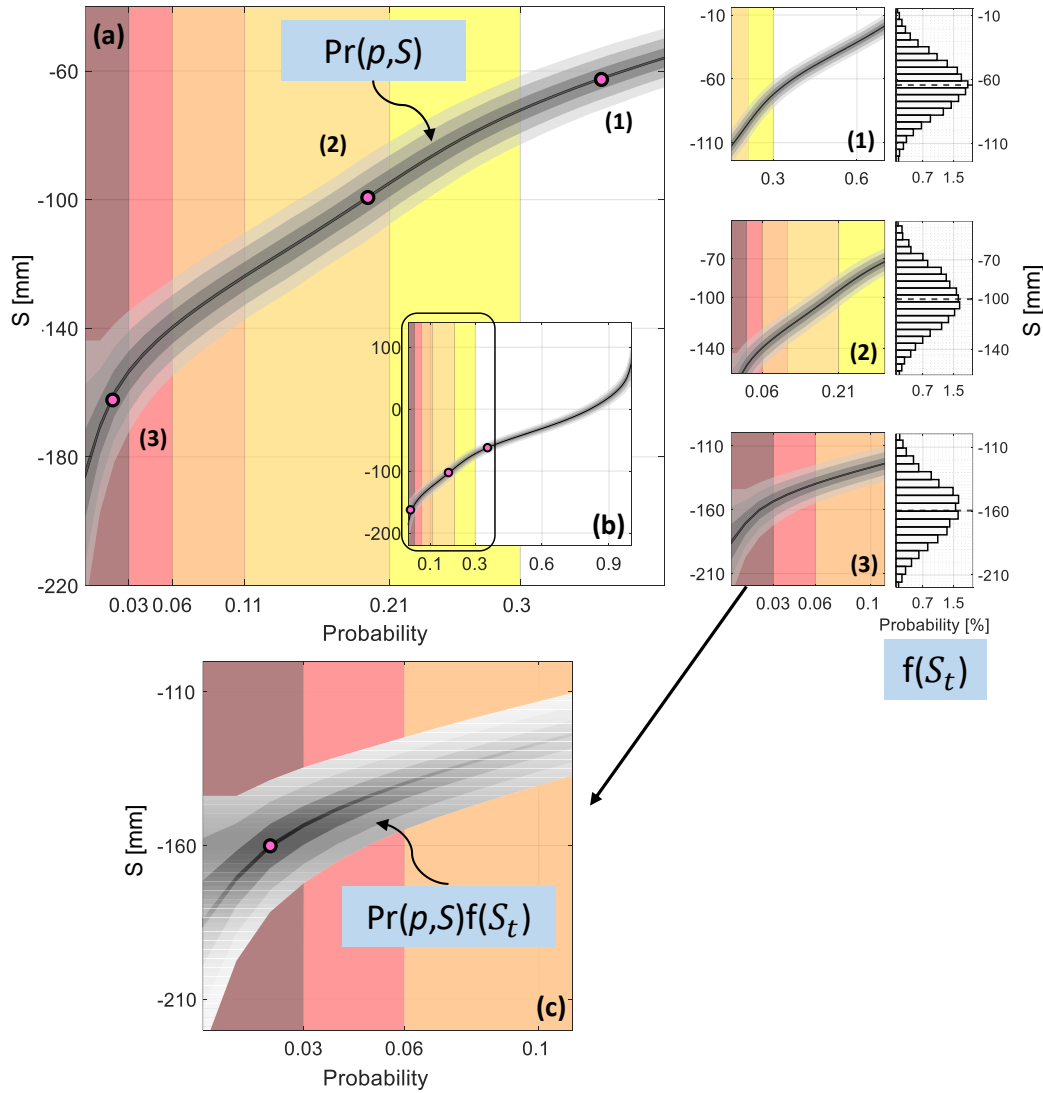


Figure 4. (a) The quantile functions (inverse of the Cumulative Distribution Function (CDF)) of the S realizations are depicted. The varying shades of gray signify the density of data points, with darker shades indicating higher density. The drought categories, ranging from D0 to D4, are delineated within their respective percentile ranges, each denoted by its corresponding color. Colored dots illustrate the positions of the three cases from Figure 3 on the quantile functions plot. These cases are further elaborated in a magnified view, accompanied by the corresponding probability distribution derived from S and its associated uncertainty. (b) Similarly, as in (a), this visualization portrays the quantile functions plot, but encompasses the complete range of quantile values. (c) The density of the counted points after integrating the probability distribution stemming from the S and its corresponding uncertainty. It's important to note that the presented results are centered on the Death Valley basin within the United States.

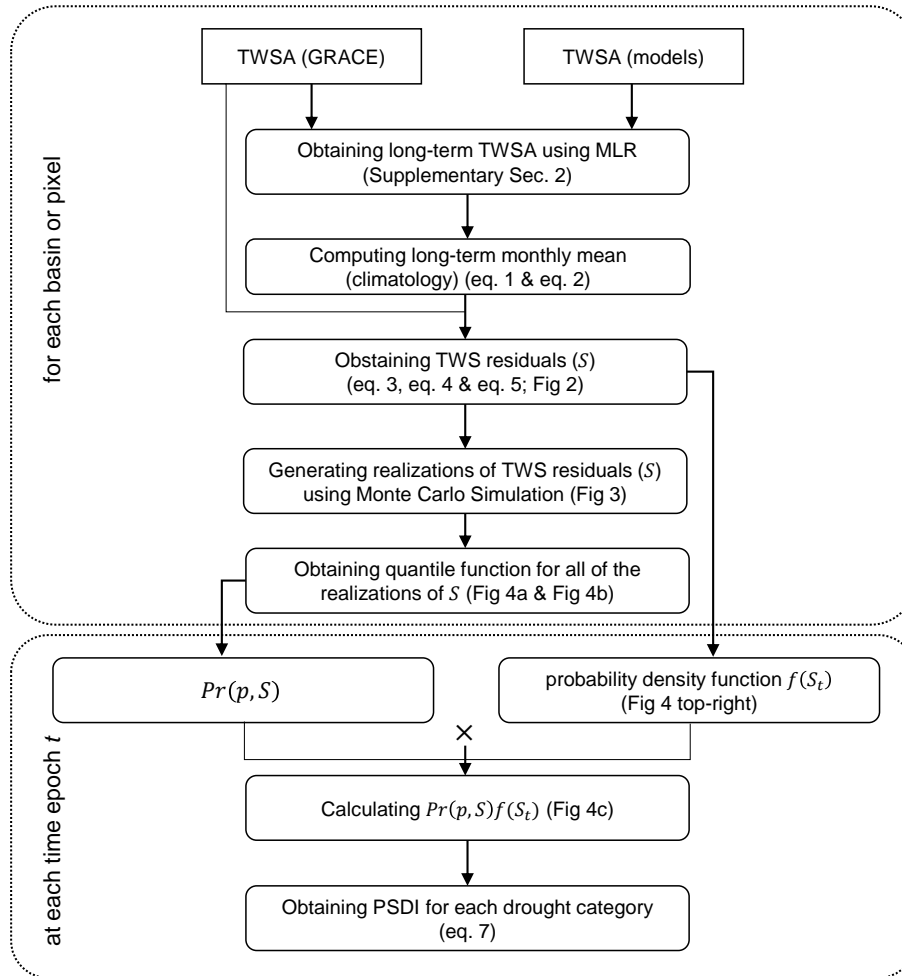


Figure 5. Flowchart of the proposed PSDI framework.

269 3 Results and Discussion

270 3.1 PSDI vs SDI

271 The PSDI approach offers a more nuanced understanding of drought conditions compared to
 272 the SDI approach. This is because PSDI captures the uncertainty associated with drought
 273 severity, while the SDI approach may oversimplify the classification of drought conditions.
 274 Although the SDI categorization is often the most probable category according to the PSDI,
 275 the neighboring categories may also have significant probabilities. This tendency becomes
 276 more pronounced as the intensity of the drought increases. This can be attributed to the

277 lower slope of the CDF curve over more severe droughts and the wider range of quantile
278 values.

279 To delve deeper into the analysis, we have quantified the disparities between drought cat-
280 egorizations as defined by SDI and PSDI_{max}—the category of drought with the highest
281 probability in PSDI—across the world’s major river basins, with the exclusion of Greenland
282 and Antarctica. The findings, illustrated in Figure 6 (a), shed light on the prevalence of
283 these discrepancies throughout the study period spanning from 2003 to 2016. The ratio
284 exhibits a range of variations, hovering near zero for basins such as Lake Balkhash in south-
285 eastern Kazakhstan or Po in Italy to a significant value of 30 % over Highland of Ethiopia
286 and Somalia in Africa or Sao Francisco in Brazil. In general, the risk of mischaracterizing
287 storage-based drought through the deterministic approach is notably high (exceeding 10 %
288 in Figure 6 (a)) across Africa (excluding the northern region), Eastern Europe, Mongolia,
289 Russia, and within the river basins of Nelson river, St. Lawrence, and Colorado (Argentina).
290 In instances where discrepancies arise between SDI and PSDI_{max}, a predominant tendency
291 is for SDI to overestimate the drought category. This is evident when comparing Figure 6
292 (b) and Figure 6 (c).

293 To investigate further, Figure 7 provides a visual comparison between two approaches for
294 characterizing drought: probabilistic (PSDI) and deterministic (SDI), over several selected
295 basins. The distribution of the basins is shown in the top panel of the Figure 7. For each
296 basin, the drought categories, ranging from the status of no drought to exceptional drought
297 (D4), are displayed in columns. The probability assigned to each category at every time
298 step is depicted using gray scale. The deterministic perspective is illustrated with red boxes,
299 allowing for a direct comparison of the two approaches.

300 The Danube and Ganges basins exhibited no disparity between SDI and PSDI_{max} from
301 2015 to 2016. In contrast, the Mississippi basin displayed the most substantial mismatch
302 between SDI and PSDI_{max}. It’s noteworthy that these mismatches were confined to adjacent
303 categories. Specifically, when considering mismatches spanning more than one category, only

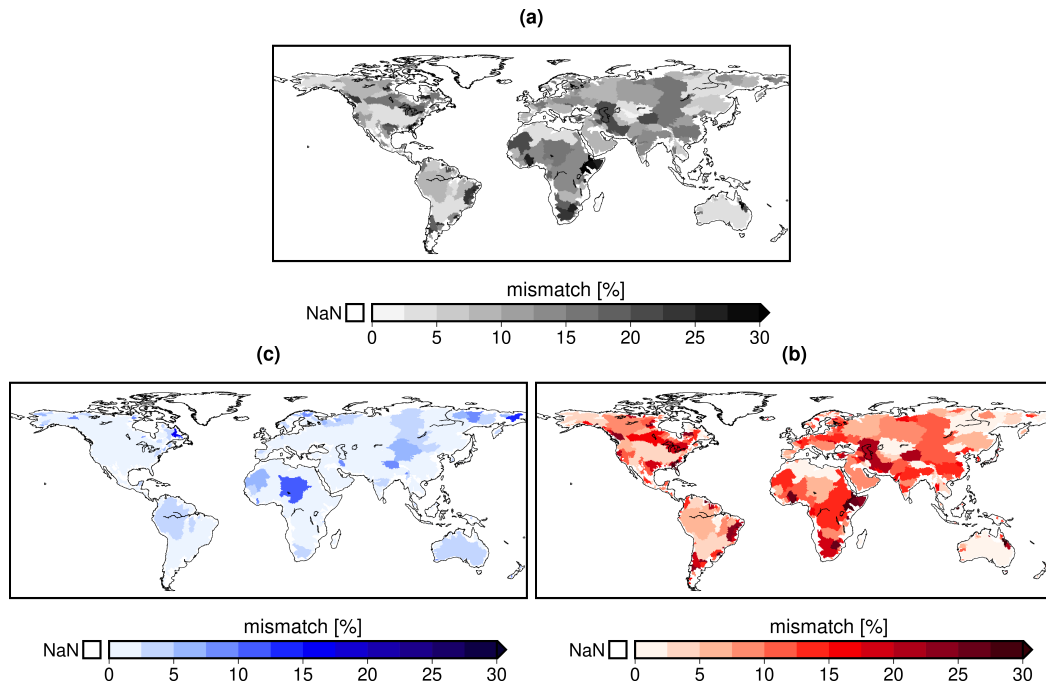


Figure 6. (a) Basin-wise distribution of the discrepancies between SDI and PSDI_{max}. The values represent the percentage of epochs where PSDI_{max} differs from SDI by at least two drought categories. (b) the percentage of epochs with a discrepancy of more than one category higher in SDI compared to PSDI_{max}. (c) the percentage of epochs with a discrepancy of more than one category lower in SDI compared to PSDI_{max}. Greenland and Antarctica are excluded from the maps.

304 four basins had such occurrences: one month in Amazonas and Nile, two months in Niger,
 305 and five months in Murray Darling. Across all basins, when a discrepancy arose between
 306 SDI and PSDI_{max}, the SDI category consistently indicated a higher severity of drought.

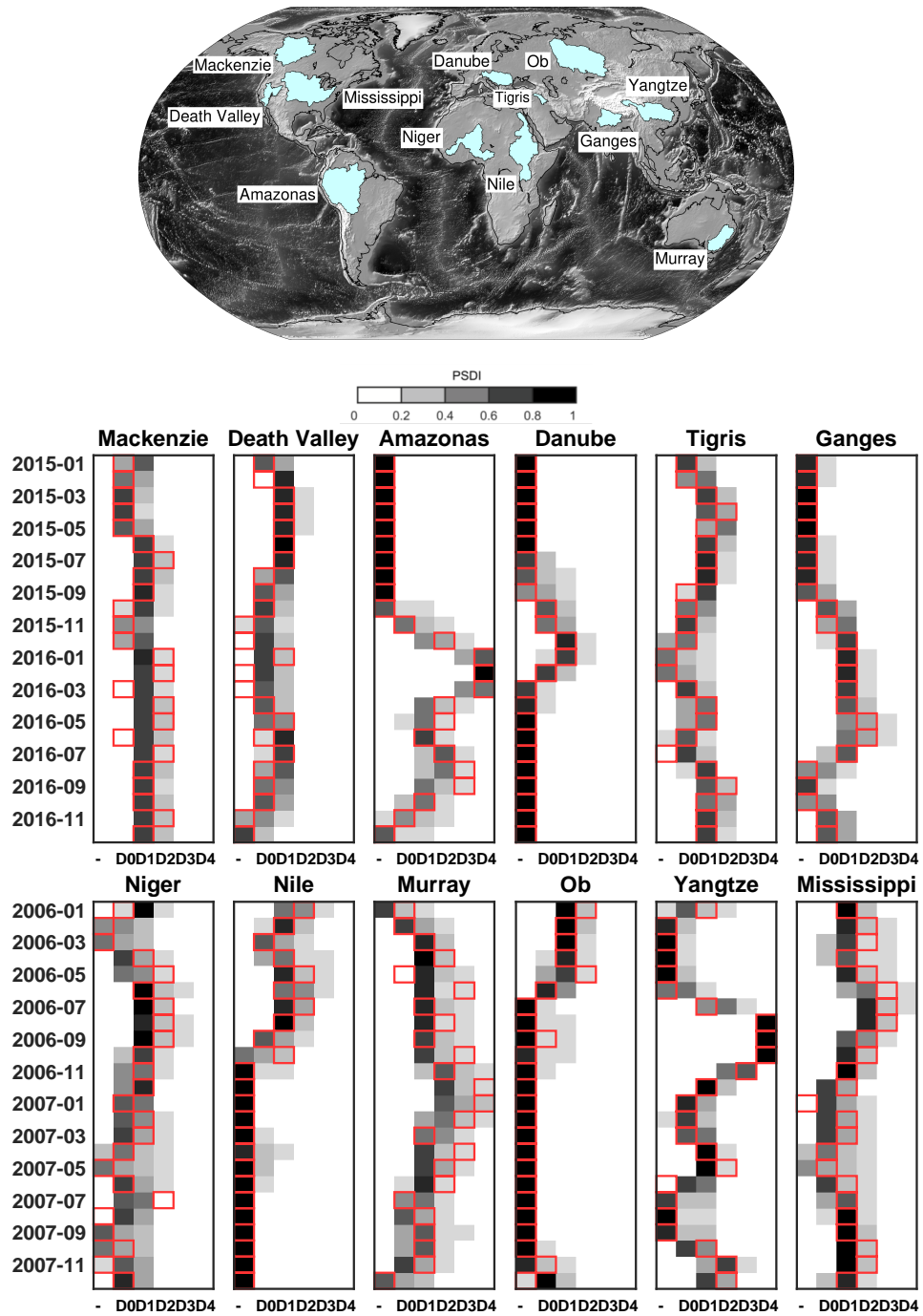


Figure 7. Top: The global distribution of the selected basins. Bottom: The SDI (red boxes) together with PSDI (gray scale probability range) for selected basins. The basins are shown in two groups considering the period with more frequency of drought, the first row between 2015–2016 and the second row between 2006–2007. The “-” represents “no drought” or “normal state” of the water storage.

307 We have investigated further the sensitivity of different categories of drought to incorpo-
 308 rating uncertainties into drought characterization. Figure 8 (a) visualizes the percentage
 309 of epochs where PSDI_{\max} differs from SDI by at least two drought categories. The results
 310 suggest that such discrepancies can diverge significantly in the categorization of drought con-
 311 ditions, especially in the D1, D2, and D3 categories, especially in D2. We have also compared
 312 the ratio of the mismatch period with respect to different climate categories (Figure 8 (b)).
 313 For more detailed information about the categories and the method of classification, please
 314 see section 4 in the supplementary file. Although the mismatch range can vary from arid to
 315 humid climate, the average value of the mismatch is the same over different climate regions,
 316 with a slightly higher value for the Dry sub-humid regions (Dry sH).

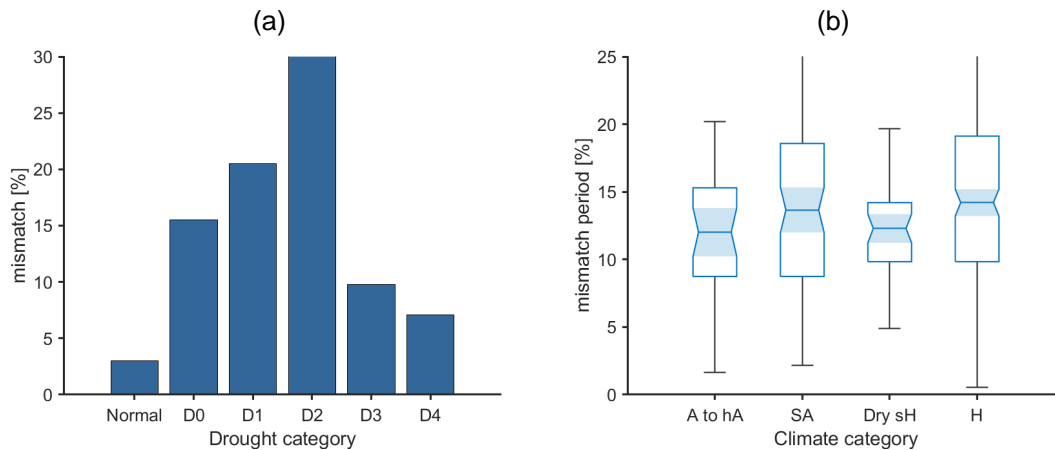


Figure 8. (a) A barplot illustrates the percentage of epochs where PSDI_{\max} diverges from SDI by at least two drought categories. (b) Boxplot of the mismatch between the PSDI_{\max} and SDI over different climate categories, namely, arid to hyper-arid (A to hA), semi-arid (SA), dry sub-humid (Dry sH), and humid (H). It is noteworthy that to count the number of months, we have considered those with more than one category difference between the PSDI_{\max} and SDI.

317 3.2 Performance of the PSDI during extreme hydrologic events

318 To assess the PSDI's reliability, we analyzed its performance during several well-documented
 319 extreme hydrologic events between 2002 and 2016. The drought events during 2012 included
 320 the moderate to exceptional drought over the United state (Boyer et al., 2013; Ault et al.,
 321 2013), southern Europe (Oikonomou et al., 2020; Spinoni et al., 2015). The drought affected

322 many Middle East regions between 2007 and 2008 (Barlow et al., 2016). Southern Africa
 323 suffered from a severe to exceptional drought between 2005 and early 2006 (Nicholson,
 324 2014), while central Argentina and Paraguay were affected by drought throughout 2009
 325 (Guha-Sapir et al., 2016). Moreover, Australia experienced the worst drought recorded
 326 since European settlement in the 2000s, called the *Millennium drought*, with a peak in
 327 2006 that affected many regions of the south to the east, including agricultural lands of
 328 the Murray-Darling basin (Van Dijk et al., 2013; Heberger, 2012). Figure 9 illustrates the
 329 performance of the PSDI over the events mentioned above. For each region, the category
 330 with the maximum probability and the estimated probability is shown for the selected
 331 date. Generally, the PSDI shows high performance in characterizing drought in the selected
 332 drought events (Figure 9). Comparing the SDI with $PSDI_{max}$ reveals that SDI categorizes
 333 higher drought intensities.

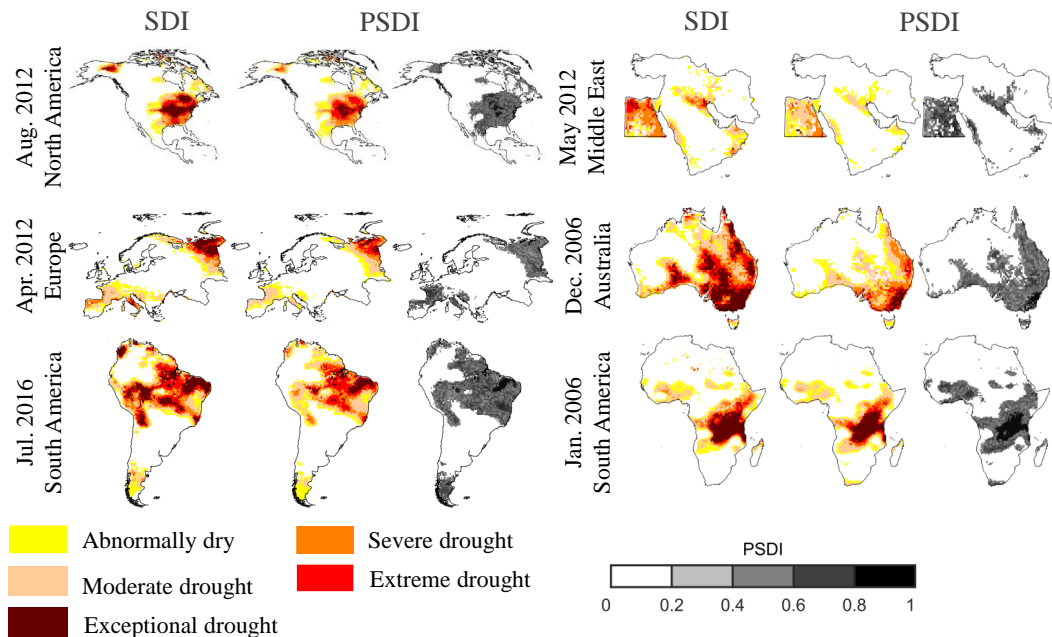


Figure 9. Comparing SDI with PSDI during some reported drought events.

334 4 Conclusions

335 For the first time, this study presents a probabilistic approach to characterizing TWS
336 drought using time-variable gravity from satellite gravimetry. Our proposed framework
337 acknowledges and addresses the inherent uncertainties associated with GRACE data. Our
338 approach leverages Monte Carlo simulations to generate realistic realizations, capturing the
339 stochastic nature of the TWSA time series. This ensemble reflects the diverse possible sce-
340 narios and their associated uncertainties, paving the way for a more insightful understanding
341 of drought conditions. We have monitored the results of the proposed PSDI over major river
342 basins and compared the result with SDI (deterministic approach). Our spatial analysis un-
343 derscores the significance of adopting a probabilistic approach. It becomes evident that
344 deterministic methodologies, in certain regions, tend to overestimate the severity of storage-
345 based drought, potentially leading to misleading conclusions. While deterministic indices
346 may tend to oversimplify drought categorization, PSDI accounts for uncertainty, thereby
347 offering a more accurate representation of drought severity, particularly during extreme
348 events.

349 Furthermore, our study assesses the performance of PSDI during well-documented extreme
350 hydrologic events, spanning from the United States to Europe, the Middle East, South-
351 ern Africa, South America, and Australia. In each case, PSDI demonstrates its robustness
352 in characterizing drought conditions. Comparing the SDI with PSDI_{\max} reveals that the
353 drought can be categorized with more intensity using SDI with respect to the PSDI. We also
354 address the uncertainties associated with different GRACE mascon products, emphasizing
355 the importance of selecting the appropriate data source for reliable drought characterization.
356 Variations in uncertainty estimates among different centers and processing methods high-
357 light the need for caution when utilizing GRACE-derived data for drought analysis. We also
358 shed light on the formal errors associated with GRACE data, highlighting the overestima-
359 tion and underestimation tendencies of various solutions. This insight serves as a valuable

360 reference for researchers and institutions relying on GRACE data for drought monitoring
361 and assessment.

362 The findings of this study underscore the importance of a probabilistic approach in charac-
363 terizing drought over various regions and during several drought events. The new approach
364 provides a more realistic characterization of drought by accounting for the uncertainties
365 in the GRACE(-FO) TWSA data in contrast to the common deterministic approach. By
366 embracing uncertainty and providing a comprehensive ensemble of drought scenarios, PSDI
367 advances the field of drought assessment, offering improved accuracy and insight for decision-
368 makers and researchers alike. In an era marked by changing climate patterns and increasing
369 water stress, our probabilistic approach represents a significant step toward more effective
370 drought management and adaptation strategies.

371 **Author Contribution Statement**

372 Peyman Saemian and Mohammad J. Tourian developed the method, conducted the data
373 analysis, and wrote the paper. Omid Elmi contributed to the analysis and assisted in pro-
374 ducing graphics. Amir Aghakouchak and Nico Sneeuw supported the study with discussions
375 on algorithm development. All authors commented on and reviewed the manuscript, and
376 contributed to the final version.

377 **Open Research**

378 In this study, we employed a diverse set of datasets. The GRACE data, the GSFC mas-
379 con product, is available at <https://earth.gsfc.nasa.gov/geo/data/grace-mascons>.
380 Nine global water resources datasets, including PCR-GLOBWB, SURFEX-TRIP, HBV-
381 SIMREG, HTESEL, JULES, LISFLOOD, ORCHIDEE, SWBM, and W3RA, were ob-
382 tained from the earthH2Observe Water Cycle Integrator (<ftp://wci.earth2observe.eu>).
383 CLM5 products are accessible via Earth System Grid (Oleson et al., 2019). The WaterGAP
384 Global Hydrology Model (WaterGAP v2.2d) data is accessible at <https://doi.pangaea>

385 .de/10.1594/PANGAEA.918447. Additionally, the fifth generation ECMWF atmospheric
386 reanalysis (ERA5) data can be downloaded from the Copernicus Climate Change Service
387 (C3S) at ECMWF (<https://cds.climate.copernicus.eu>). For the long-term TWSA
388 from the MLR approach, the data is available in mat format at DaRUS “Data for: A prob-
389 abilistic approach to characterizing drought using satellite gravimetry”, [https://doi.org/](https://doi.org/10.18419/darus-3832)
390 10.18419/darus-3832.

391 **Acknowledgments**

392 We extend our gratitude to the numerous organizations and data providers whose contri-
393 butions were essential to the success of this research. The datasets utilized in this study
394 were sourced from various centers and repositories, as comprehensively listed in Tables 1
395 and 2 of the Supplementary section 1. We acknowledge the invaluable support and data
396 access made possible by these sources. P. Saemian is funded by the DFG funding in project
397 RASLyBoCa within the Special Priority Program Regional Sea Level Change & Society
398 ‘SeaLevel’, Germany (SPP1889)—Project number 313883668, Grant TO 1042/3-1. O. Elmi
399 is funded by DFG (Deutsche Forschungsgemeinschaft) (project Number: 324641997) within
400 the framework of the Research Unit 2630, GlobalCDA: understanding the global freshwa-
401 ter system by combining geodetic and remote sensing information with modeling using a
402 calibration/data assimilation approach (<https://globalcda.de>).

403 **References**

- 404 AghaKouchak, A., Farahmand, A., Melton, F., Teixeira, J., Anderson, M., Wardlow, B.,
405 & Hain, C. (2015). Remote sensing of drought: progress, challenges and opportunities.
406 *Reviews of Geophysics*, 53(2), 452–480. (doi: 10.1002/2014RG000456)
- 407 AghaKouchak, A., Huning, L. S., Sadegh, M., Qin, Y., Markonis, Y., Vahedifard, F., ...
408 others (2023). Toward impact-based monitoring of drought and its cascading hazards.
409 *Nature Reviews Earth & Environment*, 1–14.
- 410 AghaKouchak, A., Mirchi, A., Madani, K., Di Baldassarre, G., Nazemi, A., Alborzi, A., ...

- 411 others (2021). *Anthropogenic Drought: Definition, Challenges, and Opportunities*. Wiley
 412 Online Library. doi: 10.1029/2019RG000683
- 413 Ahmadalipour, A., Moradkhani, H., Yan, H., & Zarekarizi, M. (2017). Remote sensing of
 414 drought: vegetation, soil moisture, and data assimilation. In *Remote sensing of hydrolog-
 415 ical extremes* (pp. 121–149). Springer.
- 416 Ault, T., Henebry, G., De Beurs, K., Schwartz, M., Betancourt, J. L., & Moore, D. (2013).
 417 The false spring of 2012, earliest in North American record. *Eos, Transactions American
 418 Geophysical Union, 94*(20), 181–182. doi: 10.1002/2013EO200001
- 419 Barlow, M., Zaitchik, B., Paz, S., Black, E., Evans, J., & Hoell, A. (2016). A review of
 420 drought in the Middle East and southwest Asia. *Journal of climate, 29*(23), 8547–8574.
 421 doi: 10.1175/JCLI-D-13-00692.1
- 422 Behling, R., Roessner, S., Foerster, S., Saemian, P., Tourian, M. J., Portele, T. C., & Lorenz,
 423 C. (2022). Interrelations of vegetation growth and water scarcity in Iran revealed by
 424 satellite time series. *Scientific Reports, 12*(1), 20784. doi: 10.1038/s41598-022-24712-6
- 425 Box, G. E., & Muller, M. E. (1958). A note on the generation of random normal deviates.
 426 *The annals of mathematical statistics, 29*(2), 610–611. doi: 10.1214/aoms/1177706645
- 427 Boyer, J., Byrne, P., Cassman, K., Cooper, M., Delmer, D., Greene, T., . . . others (2013).
 428 The US drought of 2012 in perspective: a call to action. *Global Food Security, 2*(3),
 429 139–143. doi: 10.1016/j.gfs.2013.08.002
- 430 Coelho, C. A., & Goddard, L. (2009). El niño–induced tropical droughts in climate change
 431 projections. *Journal of Climate, 22*(23), 6456–6476. doi: 10.1175/2009JCLI3185.1
- 432 Coumou, D., & Rahmstorf, S. (2012). A decade of weather extremes. *Nature climate change,
 433 2*(7), 491. doi: 10.1038/nclimate1452
- 434 Donat, M. G., Lowry, A. L., Alexander, L. V., O’Gorman, P. A., & Maher, N. (2016). More
 435 extreme precipitation in the world’s dry and wet regions. *Nature Climate Change, 6*(5),
 436 508. doi: 10.1038/nclimate2941
- 437 Famiglietti, J. S., Lo, M., Ho, S. L., Bethune, J., Anderson, K., Syed, T. H., . . . Rodell, M.
 438 (2011). Satellites measure recent rates of groundwater depletion in California’s Central

- 439 Valley. *Geophysical Research Letters*, *38*(3). doi: 10.1029/2010GL046442
- 440 FAO. (2021). Drought [Computer software manual]. ([http://www.fao.org/land-water/](http://www.fao.org/land-water/water/drought/en/)
441 [water/drought/en/](http://www.fao.org/land-water/water/drought/en/))
- 442 Gardner, A. S., Moholdt, G., Cogley, J. G., Wouters, B., Arendt, A. A., Wahr, J., ...
443 others (2013). A reconciled estimate of glacier contributions to sea level rise: 2003 to
444 2009. *science*, *340*(6134), 852–857. doi: 10.1126/science.1234532
- 445 Gouweleeuw, B. T., Kvas, A., Gruber, C., Gain, A. K., Mayer-Gürr, T., Flechtner, F., &
446 Güntner, A. (2018). Daily GRACE gravity field solutions track major flood events in the
447 Ganges–Brahmaputra Delta. *Hydrology and Earth System Sciences*, *22*(5), 2867–2880.
448 doi: 10.5194/hess-22-2867-2018
- 449 Guha-Sapir, D., Below, R., & Hoyois, P. (2016). EM-DAT: the CRED/OFDA international
450 disaster database. *Université Catholique de Louvain*. Retrieved from [https://www.emdat](https://www.emdat.be/)
451 [.be/](https://www.emdat.be/)
- 452 Heberger, M. (2012). Australia’s millennium drought: Impacts and responses. In *The*
453 *world’s water* (pp. 97–125). Springer.
- 454 Heim Jr, R. R. (2002). A review of twentieth-century drought indices used in the united
455 states. *Bulletin of the American Meteorological Society*, *83*(8), 1149–1166. doi: 10.1175/
456 1520-0477-83.8.1149
- 457 Hisdal, H., Stahl, K., Tallaksen, L. M., & Demuth, S. (2001). Have streamflow droughts
458 in Europe become more severe or frequent? *International Journal of Climatology*, *21*(3),
459 317–333. doi: 10.1002/joc.619
- 460 Hosseini-Moghari, S.-M., Araghinejad, S., Ebrahimi, K., Tang, Q., & AghaKouchak, A.
461 (2020). Using GRACE satellite observations for separating meteorological variability
462 from anthropogenic impacts on water availability. *Scientific Reports*, *10*(1), 15098. doi:
463 10.1038/s41598-020-71837-7
- 464 Hulme, M. (1992). A 1951–80 global land precipitation climatology for the evaluation of
465 general circulation models. *Climate dynamics*, *7*, 57–72. doi: 10.1007/BF00209609
- 466 Jiang, D., Wang, J., Huang, Y., Zhou, K., Ding, X., & Fu, J. (2014). The review of GRACE

- 467 data applications in terrestrial hydrology monitoring. *Advances in Meteorology*, 2014.
468 doi: 10.1155/2014/725131
- 469 Jones, P. D., & Hulme, M. (1996). Calculating regional climatic time series for temperature
470 and precipitation: methods and illustrations. *International Journal of Climatology: A*
471 *Journal of the Royal Meteorological Society*, 16(4), 361–377. doi: 10.1002/(SICI)1097
472 -0088(199604)16:4<361::AID-JOC53>3.0.CO;2-F
- 473 Kreibich, H., Van Loon, A. F., Schröter, K., Ward, P. J., Mazzoleni, M., Sairam, N., ...
474 others (2022). The challenge of unprecedented floods and droughts in risk management.
475 *Nature*, 608(7921), 80–86. doi: 10.1038/s41586-022-04917-5
- 476 Kvas, A., Behzadpour, S., Ellmer, M., Klingler, B., Strasser, S., Zehentner, N., & Mayer-
477 Gürr, T. (2019). ITSG-Grace2018: Overview and evaluation of a new GRACE-only
478 gravity field time series. *Journal of Geophysical Research: Solid Earth*, 124(8), 9332–
479 9344. doi: 10.1029/2019JB017415
- 480 Li, W., Pan, R., Jiang, Z., Chen, Y., Li, L., Luo, J.-J., ... Yu, J. (2021). Future changes in
481 the frequency of extreme droughts over China based on two large ensemble simulations.
482 *Journal of Climate*, 34(14), 6023–6035.
- 483 Lorenz, C., Kunstmann, H., Devaraju, B., Tourian, M. J., Sneeuw, N., & Riegger, J. (2014).
484 Large-scale runoff from landmasses: a global assessment of the closure of the hydrological
485 and atmospheric water balances. *Journal of Hydrometeorology*, 15(6), 2111–2139. doi:
486 10.1175/JHM-D-13-0157.1
- 487 Metropolis, N., & Ulam, S. (1949). The Monte Carlo method. *Journal of the American*
488 *statistical association*, 44(247), 335–341.
- 489 Mishra, A. K., & Singh, V. P. (2010). A review of drought concepts. *Journal of hydrology*,
490 391(1-2), 202–216.
- 491 Mishra, A. K., & Singh, V. P. (2011). Drought modeling—a review. *Journal of Hydrology*,
492 403(1-2), 157–175.
- 493 Mooney, C. Z. (1997). *Monte Carlo simulation* (Vol. 116). Sage publications.
- 494 Narasimhan, B., & Srinivasan, R. (2005). Development and evaluation of Soil Mois-

- 495 ture Deficit Index (SMDI) and Evapotranspiration Deficit Index (ETDI) for agricul-
496 tural drought monitoring. *Agricultural and Forest Meteorology*, *133*(1-4), 69–88. doi:
497 10.1016/j.agrformet.2005.07.012
- 498 Naumann, G., Cammalleri, C., Mentaschi, L., & Feyen, L. (2021). Increased economic
499 drought impacts in Europe with anthropogenic warming. *Nature Climate Change*, *11*(6),
500 485–491. doi: 10.1038/s41558-021-01044-3
- 501 Nicholson, S. E. (2014). A detailed look at the recent drought situation in the Greater Horn
502 of Africa. *Journal of Arid Environments*, *103*, 71–79. doi: 10.1016/j.jaridenv.2013.12.003
- 503 Oikonomou, P. D., Karavitis, C. A., Tsesmelis, D. E., Kolokytha, E., & Maia, R. (2020).
504 Drought characteristics assessment in Europe over the Past 50 Years. *Water Resources*
505 *Management*, *34*(15), 4757–4772. doi: 10.1007/s11269-020-02688-0
- 506 Oleson, K., Lawrence, D., Lombardozzi, D., & Wieder, D. (2019). *CLM land-only release*.
507 (Accessed: 2021-05-30) doi: <https://doi.org/10.5065/d6154fwh>
- 508 Palmer, W. C. (1965). *Meteorological drought* (Vol. 30). US Department of Commerce,
509 Weather Bureau.
- 510 Reager, J. T., & Famiglietti, J. S. (2009). Global terrestrial water storage capac-
511 ity and flood potential using GRACE. *Geophysical research letters*, *36*(23). doi:
512 10.1029/2009GL040826
- 513 Rodell, M., Chen, J., Kato, H., Famiglietti, J. S., Nigro, J., & Wilson, C. R. (2007). Esti-
514 mating groundwater storage changes in the Mississippi River basin (USA) using GRACE.
515 *Hydrogeology Journal*, *15*(1), 159–166. doi: 0.1007/s10040-006-0103-7
- 516 Rodell, M., Velicogna, I., & Famiglietti, J. S. (2009). Satellite-based estimates of ground-
517 water depletion in India. *Nature*, *460*(7258), 999–1002. doi: 10.1038/nature08238
- 518 Saemian, P., Elmi, O., Vishwakarma, B., Tourian, M., & Sneeuw, N. (2020). Analyzing
519 the Lake Urmia restoration progress using ground-based and spaceborne observations.
520 *Science of The Total Environment*, *739*, 139857. doi: 10.1016/j.scitotenv.2020.139857
- 521 Saemian, P., Tourian, M. J., AghaKouchak, A., Madani, K., & Sneeuw, N. (2022). How
522 much water did Iran lose over the last two decades? *Journal of Hydrology: Regional*

- 523 *Studies*, 41, 101095. doi: 10.1016/j.ejrh.2022.101095
- 524 Scholz, C. A., Johnson, T. C., Cohen, A. S., King, J. W., Peck, J. A., Overpeck, J. T.,
 525 ... others (2007). East african megadroughts between 135 and 75 thousand years ago
 526 and bearing on early-modern human origins. *Proceedings of the National Academy of*
 527 *Sciences*, 104(42), 16416–16421.
- 528 Shepherd, A., Ivins, E., Rignot, E., Smith, B., Van Den Broeke, M., Velicogna, I., ... others
 529 (2018). Mass balance of the Antarctic Ice Sheet from 1992 to 2017. *Nature*, 558, 219–222.
 530 doi: 10.1038/s41586-018-0179-y
- 531 Sinha, D., Syed, T. H., Famiglietti, J. S., Reager, J. T., & Thomas, R. C. (2017). Charac-
 532 terizing drought in India using GRACE observations of terrestrial water storage deficit.
 533 *Journal of Hydrometeorology*, 18(2), 381–396. doi: 10.1175/JHM-D-16-0047.1
- 534 Sohn, B., Yeh, S.-W., Schmetz, J., & Song, H.-J. (2013). Observational evidences of
 535 Walker circulation change over the last 30 years contrasting with GCM results. *Climate*
 536 *Dynamics*, 40, 1721–1732. doi: 10.1007/s00382-012-1484-z
- 537 Spinoni, J., Naumann, G., Vogt, J. V., & Barbosa, P. (2015). The biggest drought events
 538 in Europe from 1950 to 2012. *Journal of Hydrology: Regional Studies*, 3, 509–524. doi:
 539 10.1016/j.ejrh.2015.01.001
- 540 Sun, A. Y., Scanlon, B. R., AghaKouchak, A., & Zhang, Z. (2017). Using GRACE satellite
 541 gravimetry for assessing large-scale hydrologic extremes. *Remote Sensing*, 9(12), 1287.
 542 doi: 10.3390/rs9121287
- 543 Svoboda, M., Fuchs, B., et al. (2016). *Handbook of drought indicators and indices*. World
 544 Meteorological Organization Geneva, Switzerland.
- 545 Svoboda, M., Hayes, M., & Wood, D. (2012). *Standardized precipitation index: user guide*
 546 (Tech. Rep. No. NO. 1090).
- 547 Svoboda, M., LeComte, D., Hayes, M., Heim, R., Gleason, K., Angel, J., ... others (2002).
 548 The drought monitor. *Bulletin of the American Meteorological Society*, 83(8), 1181–1190.
- 549 Tapley, B. D., Bettadpur, S., Watkins, M., & Reigber, C. (2004). The gravity recovery
 550 and climate experiment: Mission overview and early results. *Geophysical research letters*,

- 551 31(9). doi: 10.1029/2004GL019920
- 552 Teuling, A. J. (2018). A hot future for european droughts. *Nature Climate Change*, 8(5),
553 364–365.
- 554 Thomas, A. C., Reager, J. T., Famiglietti, J. S., & Rodell, M. (2014). A GRACE-based
555 water storage deficit approach for hydrological drought characterization. *Geophysical
556 Research Letters*, 41(5), 1537–1545. doi: 10.1002/2014GL059323
- 557 Tourian, M., Reager, J., & Sneeuw, N. (2018). The total drainable water storage of the
558 Amazon river basin: A first estimate using GRACE. *Water Resources Research*, 54(5),
559 3290–3312. doi: 10.1029/2017WR021674
- 560 Tourian, M. J., Elmi, O., Shafaghi, Y., Behnia, S., Saemian, P., Schlesinger, R., & Sneeuw,
561 N. (2022). Hydrosat: geometric quantities of the global water cycle from geodetic satel-
562 lites. *Earth System Science Data*, 14(5), 2463–2486.
- 563 Tourian, M. J., Saemian, P., Ferreira, V. G., Sneeuw, N., Frappart, F., & Papa, F.
564 (2023). A copula-supported Bayesian framework for spatial downscaling of GRACE-
565 derived terrestrial water storage flux. *Remote Sensing of Environment*, 295, 113685. doi:
566 10.1016/j.rse.2023.113685
- 567 van den Broeke, M., Bamber, J., Ettema, J., Rignot, E., Schrama, E., van de Berg, W. J.,
568 ... Wouters, B. (2009). Partitioning recent Greenland mass loss. *science*, 326(5955),
569 984–986. doi: 10.1126/science.1178176
- 570 Van Dijk, A. I., Beck, H. E., Crosbie, R. S., de Jeu, R. A., Liu, Y. Y., Podger, G. M.,
571 ... Viney, N. R. (2013). The Millennium Drought in southeast Australia (2001–2009):
572 Natural and human causes and implications for water resources, ecosystems, economy,
573 and society. *Water Resources Research*, 49(2), 1040–1057. doi: 10.1002/wrcr.20123
- 574 Voss, K. A., Famiglietti, J. S., Lo, M., De Linage, C., Rodell, M., & Swenson, S. C. (2013).
575 Groundwater depletion in the Middle East from GRACE with implications for trans-
576 boundary water management in the Tigris-Euphrates-Western Iran region. *Water re-
577 sources research*, 49(2), 904–914. doi: 10.1002/wrcr.20078
- 578 Wilhite, D. A. (2000). Chapter 1 drought as a natural hazard: Concepts and definitions.

579 *Drought Mitigation Center Faculty Publications.*

580 Wilhite, D. A., Svoboda, M. D., & Hayes, M. J. (2007). Understanding the complex impacts
581 of drought: A key to enhancing drought mitigation and preparedness. *Water resources
582 management, 21*(5), 763–774. doi: 10.1007/s11269-006-9076-5

583 Yi, H., & Wen, L. (2016). Satellite gravity measurement monitoring terrestrial water storage
584 change and drought in the continental United States. *Scientific reports, 6*, 19909. doi:
585 10.1038/srep19909

586 Yi, S., Saemian, P., Sneeuw, N., & Tourian, M. J. (2023). Estimating runoff from pan-Arctic
587 drainage basins for 2002–2019 using an improved runoff-storage relationship. *Remote
588 Sensing of Environment, 298*, 113816. doi: 10.1016/j.rse.2023.113816

589 Yirdaw, S. Z., Snelgrove, K. R., & Agboma, C. O. (2008). GRACE satellite observations of
590 terrestrial moisture changes for drought characterization in the Canadian Prairie. *Journal
591 of Hydrology, 356*(1-2), 84–92. doi: 10.1016/j.jhydrol.2008.04.004

592 Yu, M., Li, Q., Hayes, M. J., Svoboda, M. D., & Heim, R. R. (2014). Are droughts becoming
593 more frequent or severe in China based on the standardized precipitation evapotranspi-
594 ration index: 1951–2010? *International Journal of Climatology, 34*(3), 545–558. doi:
595 10.1002/joc.3701

596 Zargar, A., Sadiq, R., Naser, B., & Khan, F. I. (2011). A review of drought indices.
597 *Environmental Reviews, 19*(NA), 333–349. doi: doi.org/10.1139/a11-013

598 Zhao, C., Brissette, F., Chen, J., & Martel, J.-L. (2020). Frequency change of future
599 extreme summer meteorological and hydrological droughts over north america. *Journal
600 of Hydrology, 584*, 124316.

601 Zhao, M., Geruo, A., Velicogna, I., & Kimball, J. S. (2017). A global gridded dataset
602 of GRACE drought severity index for 2002–14: Comparison with PDSI and SPEI and
603 a case study of the Australia millennium drought. *Journal of Hydrometeorology, 18*(8),
604 2117–2129. doi: 10.1175/JHM-D-16-0182.1

605 Zhong, Y., Hu, E., Wu, Y., An, Q., Wang, C., Bai, H., & Gao, W. (2023). Reconstructing
606 a long-term water storage-based drought index in the yangtze river basin. *Science of The*

607 *Total Environment*, 883, 163403.

608 Zscheischler, J., Westra, S., Van Den Hurk, B. J., Seneviratne, S. I., Ward, P. J., Pitman,

609 A., . . . others (2018). Future climate risk from compound events. *Nature Climate Change*,

610 8(6), 469–477. doi: 10.1038/s41558-018-0156-3